IJSES
Volume 9, Issue 5, pp. 7-10, 2025.
International Journal of Scientific Engineering and Science
ISSN (Online): 2456-7361

An Efficient High-Order Numerical Method for Second-Order Steklov Problem in a Sectorial Domain

Huayu Huang[1], Jihui Zheng[1,*]
[1]School of Mathematics Science, Guizhou Normal University, Guiyang 550025, China

Abstract— *In this paper, we present a spectral Galerkin method for solving the second-order Steklov eigenvalue problem in a sectorial domain. First, by using affine coordinate transformations, we reformulate the original problem into equivalent system on a rectangular domain. Then, we establish its variational and discrete forms. Finally, numerical experiments are presented to demonstrate efficiency and spectral accuracy of the proposed algorithm.*

Keywords— *Steklov eigenvalue problem, Legendre-Galerkin method, sectorial domain.*

I. INTRODUCTION

Steklov eigenvalue problems have important physical background and possesses broad applications across multiple fields [1-3]. Extensive researches have been conducted in both theoretical analysis and numerical computation. Tan et al investigated positivity preserving property across various domains [4-6], and the properties of the first eigenvalue have been explored in the literatures [7-10]. On the numerical side, numerous methods have been developed [11-14], existing works mainly focuses on solving the second-order Steklov eigenvalue problems on the rule regions. Notably, investigations of such problems in sector-shaped domains remain absent from the existing literatures.

Therefore, this paper presents a numerical method for solving second-order Steklov eigenvalue problems in sector-shaped domains. First, by employing affine transformation, we reformulate the original problem into equivalent system. Then through the construction of some weighted Sobolev spaces, we derive the weak formulation and its corresponding discrete scheme. Finally, extensive computational experiments demonstrate the algorithm's astringency and efficiency.

The rest of this paper is organized as follows: In Section 2, a weak form and its discrete scheme of the second-order Steklov eigenvalue problem are derived. In Section 3, we derive the corresponding matrix format for the discrete scheme. In Section 4, we present a series of numerical examples to validate the proposed method. Finally, we conclude the paper in Section 5.

II. EQUIVALENT COUPLED SYSTEM

We consider the following second-order Steklov problem:

$$\begin{cases} -\Delta w + w = 0, (x,y) \in \Omega, \\ \dfrac{\partial w}{\partial n} = \lambda w, (x,y) \in \partial\Omega, \end{cases} \tag{2.1}$$

where $\frac{\partial w}{\partial n}$ is the outward normal derivative on $\partial\Omega$, and $\Omega = \{(x,y) \in \mathbb{R}^2 : x = r\cos\theta,\ y = r\sin\theta,\ 0 \le r \le R,\ \theta_1 \le \theta \le \theta_2\}$.

It is clear that the weak form of (2.1) is as follows: Find $(\lambda, w) \in \mathbb{R} \times H^1(\Omega)$, such that

$$A(w,v) = \lambda B(w,v),\ v \in H^1(\Omega), \tag{2.2}$$

where

$$A(w,v) = \int_\Omega \nabla w \nabla v + wv dxdy,\ B(w,v) = \int_{\partial\Omega} wv ds.$$

Define a Laplace operator:

$$\hat{\mathrm{L}} = \frac{1}{r}\left[\partial_r(r\partial_r) + \frac{1}{r}\partial_\theta^2\right]. \tag{2.3}$$

Let $\hat{\psi}(r,\theta) = w(x,y)$. Using the chain rule for derivatives of composite functions, we can derive the equivalent form of the gradient operator as follows:

$$\nabla w = (\cos\theta\partial_r\hat{\psi} - \frac{1}{r}\sin\theta\partial_\theta\hat{\psi}, \sin\theta\partial_r\hat{\psi} + \frac{1}{r}\cos\theta\partial_\theta\hat{\psi}).$$

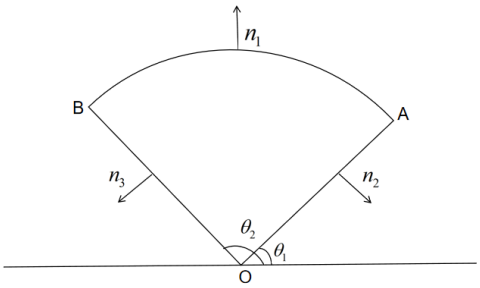

Figure 1: Sector diagram.

As shown in the Figure 1, we denote the unit outward normal vector of the arc boundary AB as $n_1 = (\cos\theta, \sin\theta)$, the unit outward normal vector of the initial boundary OA as $n_2 = (\sin\theta_1, -\cos\theta_1)$, and the unit outward normal vector of the final boundary OB as $n_3 = (-\sin\theta_2, \cos\theta_2)$. From $\frac{\partial w}{\partial n} = \nabla w \cdot n$, we deduce that (2.1) has the following equivalent form:

$$\begin{cases} -\hat{\mathrm{L}}\hat{\psi} + \hat{\psi} = 0, & (r,\theta) \in \mathrm{D}, \\ \partial_\theta\hat{\psi}(0,\theta) = 0, \partial_r\hat{\psi}(R,\theta) = \lambda\hat{\psi}(R,\theta), \theta \in (\theta_1,\theta_2), \\ -\dfrac{1}{r}\partial_\theta\hat{\psi}(r,\theta_1) = \lambda\hat{\psi}(r,\theta_1), & r \in (0,R), \\ \dfrac{1}{r}\partial_\theta\hat{\psi}(r,\theta_2) = \lambda\hat{\psi}(r,\theta_2), & r \in (0,R). \end{cases} \tag{2.4}$$

Note that $\partial_\theta\hat{\psi}(0,\theta) = 0$ is an essential polar condition and $\mathrm{D} = (0,R)\times(\theta_1,\theta_2)$.

Let

IJSES
International Journal of Scientific Engineering and Science
Volume 9, Issue 5, pp. 7-10, 2025. ISSN (Online): 2456-7361

$$r=\frac{R(1+t)}{2},\theta=\frac{a+b\vartheta}{2},(t,\vartheta)\in D=(-1,1)^2,$$

$$\mathrm{L}=\frac{1}{1+t}\partial_t[(1+t)\partial_t]+\frac{4}{b^2}\frac{1}{(1+t)^2}\partial_\vartheta^2, a=\theta_1+\theta_2, b=\theta_2-\theta_1.$$

Denoting $\psi(t,\vartheta)=\hat{\psi}(r,\theta)$, we further reformulate (2.4) as:

$$\begin{cases}-\mathrm{L}\psi+\frac{R^2}{4}\psi=0, & (t,\vartheta)\in D,\\ \partial_\vartheta\psi(-1,\vartheta)=0,\partial_t\psi(1,\vartheta)=\lambda\frac{R}{2}\psi(R,\vartheta),\vartheta\in(-1,1),\\ -\frac{1}{1+t}\partial_\vartheta\psi(t,-1)=\lambda\frac{bR}{4}\psi(t,-1), & t\in(-1,1),\\ \frac{1}{1+t}\partial_\vartheta\psi(t,1)=\lambda\frac{bR}{4}\psi(t,1), & t\in(-1,1).\end{cases} \tag{2.5}$$

We define the following non-uniformly weighted Sobolev spaces:

$$L^2_\omega(D):=\left\{\psi:\int_D\omega|\psi|^2\,dtd\vartheta<\infty\right\},\omega=\frac{b}{2}(1+t),$$

$$H^1_*(D):=\left\{\psi:\int_D\omega\partial_t\psi\partial_t h+\omega^{-1}\partial_\vartheta\psi\partial_\vartheta h+\omega\psi h dtd\vartheta<\infty,\partial_\vartheta\psi(-1,\vartheta)=0\right\},$$

the corresponding inner product and norm are given by

$$(\psi,h)_{*,1}=\int_D\omega\partial_t\psi\partial_t h+\omega^{-1}\partial_\vartheta\psi\partial_\vartheta h+\omega\psi h dtd\vartheta,$$

$$\|\psi\|_{*,1}=\sqrt{(\psi,\psi)_{*,1}}.$$

According to (2.2), a weak form of (2.5) is: Find $(\lambda,\psi)\in\mathbb{R}\times H^1_*(D)$, such that

$$\mathrm{A}(\psi,h)=\lambda\mathrm{B}(\psi,h),\ h\in H^1_*(D), \tag{2.6}$$

where

$$\mathrm{A}(\psi,h)=\int_D\omega\partial_t\psi\partial_t h+\omega^{-1}\partial_\vartheta\psi\partial_\vartheta h dtd\vartheta+\frac{bR^2}{8}\int_D(1+t)\psi h dtd\vartheta,$$

$$\mathrm{B}(\psi,h)=\frac{bR}{2}\int_{-1}^1\psi(1,\vartheta)h(1,\vartheta)d\vartheta+\frac{R}{2}\int_{-1}^1\psi(t,-1)h(t,-1)+\psi(t,1)h(t,1)dt.$$

Define an approximation space $X_N=(P_N\times P_N)\cap H^1_*(D)$. Then, the discrete scheme corresponding to (2.6) is: Find $(\lambda_N,\psi_N)\in\mathbb{R}\times X_N$, such that

$$\mathrm{A}(\psi_N,h_N)=\lambda_N\mathrm{B}(\psi_N,h_N),\forall h_N\in X_N. \tag{2.7}$$

III. Algorithmic Implementation

In this section, we shall derive the equivalent matrix form of the discrete format (2.7). Let

$$\phi_i(t)=L_i(t)-L_{i+2}(t),0\le i\le N-2,\phi_{N-1}(t)=\frac{t+1}{2},\phi_N(t)=1,$$

$$\hat{\phi}_i(\vartheta)=L_i(\vartheta)-L_{i+2}(\vartheta),0\le i\le N-2,\hat{\phi}_{N-1}(\vartheta)=L_0(\vartheta),\hat{\phi}_N(\vartheta)=L_1(\vartheta),$$

$$S_N=\mathrm{span}\{\phi_0(t),\phi_1(t),\cdots,\phi_N(t)\},\hat{S}_N=\mathrm{span}\{\hat{\phi}_0(\vartheta),\hat{\phi}_1(\vartheta),\cdots,\hat{\phi}_N(\vartheta)\}.$$

Then the approximate space is:

$$X_N=S_N\times\hat{S}_N.$$

Let us expand ψ_N as follows:

$$\psi_N=\sum_{i,j=0}^N u_{ij}\phi_i(t)\hat{\phi}_j(\vartheta). \tag{3.1}$$

We denote by

$$\mathrm{U}=\begin{pmatrix}u_{00}&u_{01}&\cdots&u_{0N}\\ u_{10}&u_{11}&\cdots&u_{1N}\\ \vdots&\vdots&\ddots&\vdots\\ u_{N0}&u_{N1}&\cdots&u_{NN}\end{pmatrix}.$$

Let $\bar{U}$ be a column vector of a length $(N+1)^2$ obtained by expanding U. Denote

$$e_{kj}=\int_{-1}^1\hat{\phi}_j(\vartheta)\hat{\phi}_k(\vartheta)d\vartheta,g_{kj}=\int_{-1}^1\hat{\phi}'_j(\vartheta)\hat{\phi}'_k(\vartheta)d\vartheta,m_{kj}=\hat{\phi}_j(-1)\hat{\phi}_k(-1),$$

$$p_{kj}=\hat{\phi}_j(1)\hat{\phi}_k(1),q_{kj}=\phi_j(1)\phi_k(1),\hat{e}_{kj}=\int_{-1}^1\phi_j(t)\phi_k(t)dt,\hat{g}_{kj}=\int_{-1}^1\frac{1}{1+t}\phi_j(t)\phi_k(t)dt,$$

$$\hat{m}_{kj}=\int_{-1}^1(1+t)\phi_j(t)\phi_k(t)dt,\hat{p}_{kj}=\int_{-1}^1(1+t)\phi'_j(t)\phi'_k(t)dt.$$

By substituting (3.1) into (2.7), and then allowing h_N across all basis functions in X_N, we obtain the following linear eigenvalue system:

$$W_1\bar{U}=\lambda_N W_2\bar{U},,$$

where

$$W_1=\frac{b}{2}E(k,:)\otimes\hat{P}(l,:)+\frac{2}{b}G(k,:)\otimes\hat{G}(l,:)+\frac{bR^2}{8}E(k,:)\otimes\hat{M}(l,:),$$

$$W_2=\frac{bR}{2}E(k,:)\otimes Q(l,:)+\frac{R}{2}(M+P)(k,:)\otimes\hat{E}(l,:),$$

$$E=(e_{ij})_{i,j=0}^N,G=(g_{ij})_{i,j=0}^N,M=(m_{ij})_{i,j=0}^N,P=(p_{ij})_{i,j=0}^N,Q=(q_{ij})_{i,j=0}^N,$$

$$\hat{E}=(\hat{e}_{ij})_{i,j=0}^N,\hat{G}=(\hat{g}_{ij})_{i,j=0}^N,\hat{M}=(\hat{m}_{ij})_{i,j=0}^N,\hat{P}=(\hat{p}_{ij})_{i,j=0}^N.$$

IV. Numerical Experiment

In this section, a series of numerical experiments will be presented to demonstrate the efficiency and spectral accuracy of our algorithm. Our program is compiled and executed in MATLAB R2016b.

Example 1: We take $R=1,\theta_1=30°,\theta_2=90°$. In Table 1, we list the first four approximate eigenvalues $\lambda_N^i(i=1,2,3,4)$ for varying values of N. To further validate the computational efficiency of our algorithm, we used the numerical solution obtained at $N=60$ as a reference value. In Figure 2, we plotted the error curves of the eigenvalues for different values of N. Additionally, in Figure 3, we presented the image of the eigenfunction corresponding to the minimum eigenvalue at $N=60$, along with the error image between the eigenfunctions corresponding to the minimum eigenvalues at $N=50$ and $N=60$.

TABLE 1. The numerical results of the first four eigenvalues for different N.

N	λ_N^1	λ_N^2	λ_N^3	λ_N^4
10	0.167847123435502	1.358638641239197	1.792266897280079	4.040399080553113
20	0.167847123322805	1.358638633801590	1.792266818716613	4.040398943579751

International Journal of Scientific Engineering and Science
Volume 9, Issue 5, pp. 7-10, 2025. ISSN (Online): 2456-7361

30	0.167847123322203	1.358638633763011	1.792266818381912	4.040398942918160
40	0.167847123322178	1.358638633761443	1.792266818369035	4.040398942891494
50	0.167847123322176	1.358638633761276	1.792266818367811	4.040398942888904

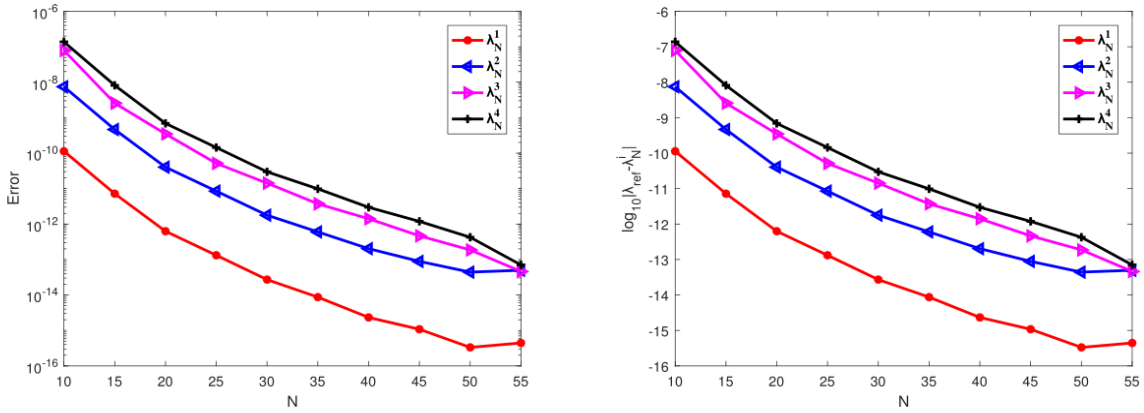

Figure 2: Error curves (left) between the numerical eigenvalues and the reference eigenvalues and their error curves (right) under semi-log scale.

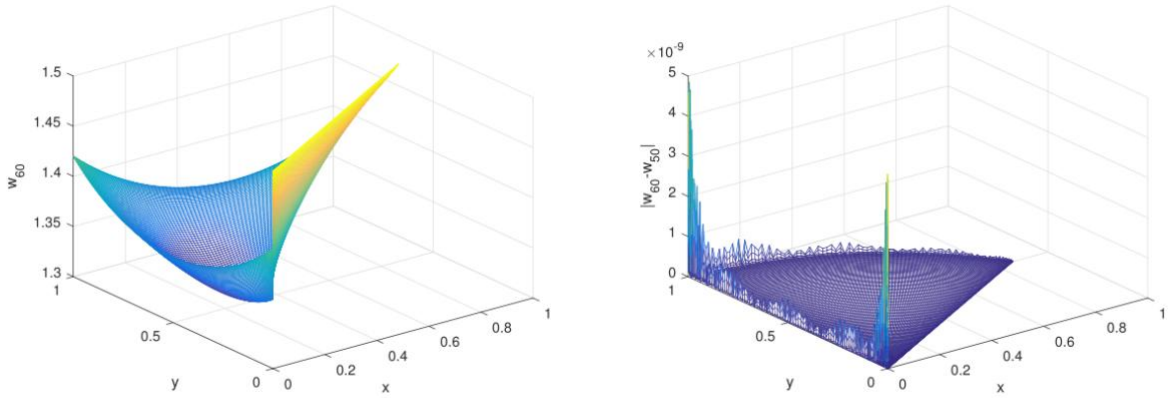

Figure 3: Image (left) of the eigenfunction $w_{60}(x,y)$ and the error image (right) between eigenfunctions $w_{60}(x,y)$ and $w_{50}(x,y)$ corresponding to the minimum eigenvalue.

As observed in Table 1, the computed eigenvalues achieve a precision of at least 10-digit when $N \geq 30$. Additionally, as illustrated in Figures 2-3, our algorithm demonstrates both convergence and spectral accuracy.

Example 2. We take $R=1, \theta_1 = 60^\circ, \theta_2 = 180^\circ$. In Table 1, we list the first four approximate eigenvalues $\lambda_N^i (i=1,2,3,4)$ for varying values of N. We used the numerical solution obtained at $N=60$ as a reference value to further validate the computational efficiency of our algorithm. In Figure 4, we plotted the error curves of the eigenvalues for different values of N. Additionally, in Figure 5, we presented the image of the eigenfunction corresponding to the minimum eigenvalue at $N=60$, along with the error image between the eigenfunctions corresponding to the minimum eigenvalues at $N=50$ and $N=60$.

As observed in Table 2, the computed eigenvalues achieve a precision of at least 10-digit when $N \geq 40$. Additionally, as illustrated in Figures 4-5, our algorithm demonstrates both convergence and spectral accuracy.

TABLE 2. The numerical results of the first four eigenvalues for different N.

N	λ_N^1	λ_N^2	λ_N^3	λ_N^4
10	0.245318192635769	1.054242994892192	2.094981780998436	2.497636674150089
20	0.245318191456520	1.054242728944644	2.094981574949448	2.497636503216148
30	0.245318191449657	1.054242726021611	2.094981573880636	2.497636502299467
40	0.245318191449364	1.054242725798506	2.094981573835764	2.497636502261011
50	0.245318191449334	1.054242725762994	2.094981573831236	2.497636502257186

International Journal of Scientific Engineering and Science
Volume 9, Issue 5, pp. 7-10, 2025. ISSN (Online): 2456-7361

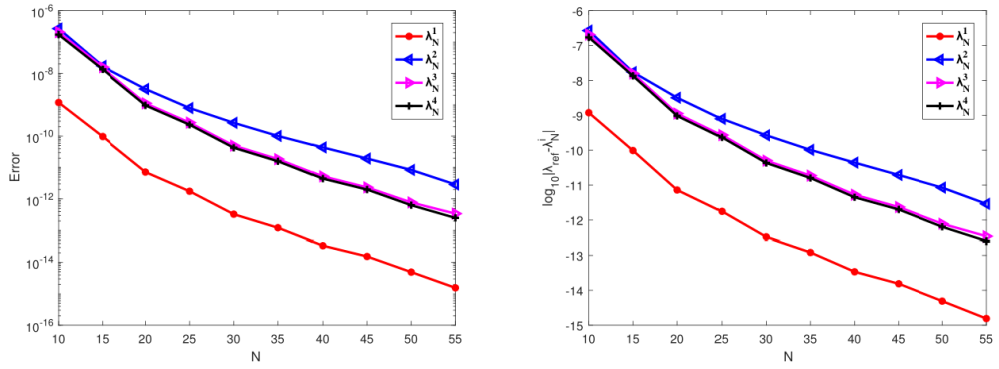

Figure 4: Error curves (left) between the numerical eigenvalues and the reference eigenvalues and their error curves (right) under semi-log scale.

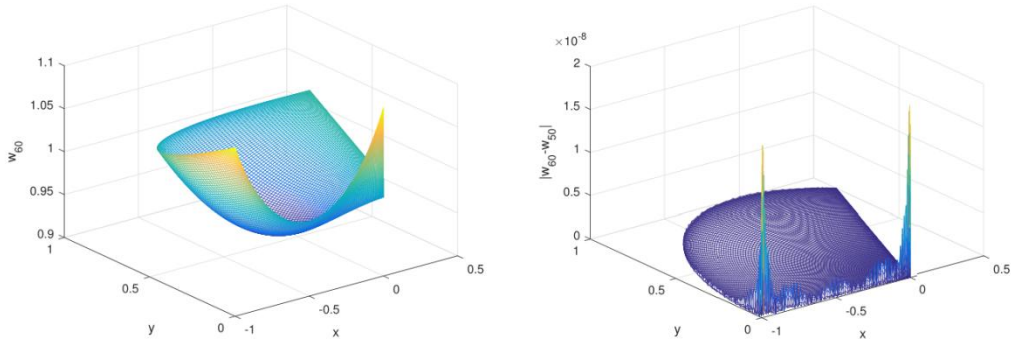

Figure 5: Image (left) of the eigenfunction $w_{60}(x, y)$ and the error image (right) between eigenfunctions $w_{60}(x, y)$ and $w_{50}(x, y)$ corresponding to the minimum eigenvalue.

V. Conclusion

In this paper, an efficient Legendre spectral method is proposed and studied for second-order Steklov eigenvalue problems in sectorial domain. By utilizing affine technology, a fresh weak formulation and its corresponding discrete variational form are formulated. In addition, numerical results validate the effectiveness of the algorithm. The algorithm proposed in this paper can also be generalized to eigenvalue problems on more complex geometric domains, which is the goal of our future research.

References

[1] Bergman, Stefan, Menahem Schiffer. Kernel functions and elliptic differential equations in mathematical physics. Courier Corporation, 2005.
[2] Alfredo Bermudez, Rodolfo Rodriguez, Duarte Santamarina. A finite element solution of an added mass formulation for coupled fluid-solid vibrations. Numerische Mathematik, 2000, 87(2): 201-227.
[3] Dorin Bucur, Ioan R. Ionescu. Asymptotic analysis and scaling of friction parameters. Zeitschrift fur angewandte Mathematik und Physik, 2006, 57(6): 1042-1056.
[4] Tan Ting, An Jing. Spectral Galerkin approximation and rigorous error analysis for the Steklov eigenvalue problem in circular domain. Mathematical Methods in the Applied Sciences, 2018, 41(10): 3764-3778.
[5] Xie Jiali, Bi Hai. A multigrid discretization scheme based on the shifted inverse iteration for the Steklov eigenvalue problem in inverse scattering. Open Mathematics, 2023, 21(1): 20220607.
[6] Oudet Edouard, Kao ChiuYen, Osting Braxton. Computation of free boundary minimal surfaces via extremal Steklov eigenvalue problems. ESAIM: Control, Optimisation and Calculus of Variations, 2021, 27: 34.
[7] James R. Kuttler. Remarks on a Stekloff Eigenvalue Problem. SIAM Journal on Numerical Analysis, 2006, 9(1): 1-5.
[8] Dorin Bucur, Filippo Gazzola. The First Biharmonic Steklov Eigenvalue: Positivity Preserving and Shape Optimization. Milan Journal of Mathematics, 2011, 79(1): 247-258.
[9] Raulot Simon, Alessandro Savo. On the first eigenvalue of the Dirichlet-to-Neumann operator on forms. Journal of Functional Analysis, 2012, 262(3): 889-914.
[10] Deng Haiyun, Yin Jiabin. The overdetermined problem and lower bound estimate on the first nonzero Steklov eigenvalue of p-Laplacian. Annali di Matematica Puraed Applicata, 2022, 201(5): 1-17.
[11] Han Xiaole, Li Yu, Xie Hehu. A Multilevel Correction Method for Steklov Eigenvalue Problem by Nonconforming Finite Element Methods. Numerical Mathematics: Theory, Methods and Applications, 2015, 8(3): 383-405.
[12] Zhang Xuqing, Yang Yidu, Bi Hai. Spectral Method with the Tensor-Product Nodal Basis for the Steklov Eigenvalue Problem. Mathematical Problems in Engineering, 2013, 2013(1): 650530.
[13] Weaam Alhejaili, Chiu-Yen Kao. Numerical studies of the Steklov eigenvalue problem via conformal mappings. Applied Mathematics and Computation, 2019, 347: 785-802..
[14] Xiong Chunguang, Xie Manting, Luo Fusheng, Su Hongling. A posteriori and superconvergence error analysis for finite element approximation of the Steklov eigenvalue problem. Computers and Mathematics with Applications, 2023, 144: 90-99.